Electronic Supplementary Material (ESI) for Nanoscale.

A universal synthesis strategy of ternary Pd-based nanowires for efficient alcohol electrooxidation

Liang Ji, [a] Xiaoyue Zhang, [b] Ningkang Qian, [a] Junjie Li, [a] Sudan Shen,[d] Xingqiao Wu, *, [b] Xin Tan, *, [b e] Hui Zhang,*, [a c] Deren Yang [a]

[a]State Key Laboratory of Silicon Materials and School of Materials Science and Engineering, Zhejiang University, Hangzhou, Zhejiang 310027, People's Republic of China.

[b]Institute for Carbon Neutralization, College of Chemistry and Materials Engineering, Wenzhou University, Wenzhou, Zhejiang 325035, People's Republic of China.

[c]Zhejiang Provincial Key Laboratory of Power Semiconductor Materials and Devices, ZJU-Hangzhou Global Scientific and Technological Innovation Center, Hangzhou, Zhejiang 311200, People's Republic of China.

[d]State Key Laboratory of Chemical Engineering, Zhejiang University, Hangzhou, Zhejiang 310027, People's Republic of China.

[e]Integrated Materials Design Laboratory, Department of Materials Physics, Research School of Physics, Australian National University, Canberra, ACT 2601, Australia

*Correspondence to: msezhanghui@zju.edu.cn, xintan@wzu.edu.cn, xingqiaowu@wzu.edu.cn

Experiments

Materials and chemicals

Sodium tetrachloropalladate (Na_2PdCl_4), bismuth triacetate ($C_6H_9BiO_6$), platinum bis(acetylacetonate) ($C_{10}H_{14}O_{14}Pt$), polyvinylpyrrolidone (PVP, M.W. ≈ 29000), cupric (II) acetylacetonate ($C_{10}H_{14}CuO_4$), cobalt (II) acetylacetonate ($C_{10}H_{16}CoO_4$), ruthenium (II) 2,4-pentanedionate ($C_{15}H_{21}O_6Ru$), dipotassium hexachloroiridate (Na_3IrCl_6) are all purchased from Sigma Aldrich. N, N-Dimethylformamide (DMF) and ethylene glycol (EG) were purchased from Sinopharm Chemical Reagent Co., Ltd. (China). All the reagents were used without further purification.

Preparation of PdBiM nanowires (NWs)

In a standard procedure, 10 mg Na_2PdCl_4, 2 mg $C_6H_9BiO_6$, 2 mg $Pt(acac)_2$ and 100 mg PVP were dissolved in a 20 ml glass vial with a mix solution of 5 ml DMF and 5 ml EG at room temperature. Then the vial was capped and transferred into an oil bath maintaining at 150 °C for 3 h. The resulting products were collected by centrifugation. PdBiPt NWs with different atomic ratios were produced by the same method except for changing the usage of $Pt(acac)_2$ (1 mg for $Pd_{84}Bi_{11}Pt_5$ NWs and 3 mg for $Pd_{77}Bi_{10}Pt_{13}$ NWs). The PdBiCo, PdBiCu, PdBiIr and PdBiRu NWs were obtained by substituting $Pt(acac)_2$ with 1.3 mg $Co(acac)_2$, 1.3 mg $Cu(acac)_2$, 2.4 mg Na_3IrCl_6 and 2 mg $Ru(acac)_3$ while maintain the other conditions.

Characterizations

The transmission electron microscope (TEM), high-resolution TEM (HRTEM) and high-angle annular dark-field scanning transmission electron microscope (HADDF-STEM) images were obtained by Hitachi HT-7700, FEI Tecnai F20 G2 and FEI titan ChemiSTEM, respectively. The X-ray diffraction (XRD) results were obtained by Bruker D8 with copper Kα radiation. The X-ray photoelectron spectrometer (XPS) was characterized on Axis Supra (Kratos Inc) with Al Kα radiation. The inductively coupled plasma atomic emission spectrometry (ICP-AES) was carried on Thermofisher ICAP

PRO X.

Electrochemical measurements

All the electrochemical measurements were carried on CHI 760E (Shanghai Chenhua Co., Ltd) with a three-electrode cell. A glassy carbon electrode (GCE) with the area of 0.196 cm^2, a Pt wire and a saturated calomel electrode (SCE) were employed as working electrode, counter electrode and reference electrode, respectively. Before the test, the catalyst was loaded on carbon support (Cabot, XC-72R). The loading weight of noble metal on the GCE is 2 μg. The EOR measurements were conducted in Ar-saturated 1 M KOH + 1 M ethanol solution, and cyclic voltammetry (CV) was carried on with the scanning range between 0.2 ~ 1.2 V vs. RHE at the scanning rate of 50 mV/s. The electrochemical active surface area (ECSA) was conducted in CO-saturated 1M KOH solution and CV curves were measured between 0-1 V vs. RHE at the scanning rate of 50 mV/s. The ECSA can be calculated according to the equation:

$$ECSA = \frac{Qco}{0.42mC/cm^2 \times mPd}$$

Electrochemical in-situ FTIR analysis

The FTIR spectrum was carried out on Bruker vertex 70V with nitrogen-cooled MCT-A detector by internal reflection method. The catalyst was first sprayed on the silicon crystal working electrode with a thin Au film. A platinum wire and a standard calomel electrode (SCE) were used as counter electrode and reference electrode. Then EOR was conducted in 1 M KOH and 1 M ethanol solution in a homemade cell. All of the spectrums were collected with 64 interferograms with a resolution of 4 cm^{-1}.

DFT calculations.

All of the spin-polarized DFT calculations were performed using the VASP program,[1-3] which uses a plane-wave basis set and a projector augmented wave method (PAW) for the treatment of core electrons.[1] The Perdew, Burke, and Ernzerhof exchange-correlation functional within a generalized gradient approximation (GGA-PBE)[4] was

used in our calculations, and the van der Waals (vdW) correction proposed by Grimme (DFT-D3)[5] was employed due to its good description of long-range vdW interactions. For the expansion of wavefunctions over the plane-wave basis set, a converged cutoff was set to 450 eV. For Pt(111) and Pd(111) surfaces, we used periodic (4 × 4) surface slabs, which contain four atomic layers with the bottom two layers fixed in their respective bulk positions and all the other atoms fully relaxed, as shown in Figure 1. The high-entropy alloys (HEA) (111) surface was constructed based on Pd(111) surface, and some Pd atoms were replaced by Pt and Bi atoms. The ratio of Pd, Pt and Bi in HEA(111) is 6:1:1. The vacuum space was set to 15 Å in the z direction to avoid interactions between periodic images. In geometry optimizations, all the structures were relaxed up to the residual atomic forces smaller than 0.01 eV/Å, and the total energy was converged to 10^{-5} eV. The Brillouin zone integration was performed on the (4×4×1) Monkhorst–Pack k-point mesh.[6] The adsorption energy of CO on metal surfaces was calculated as $E_{ads}(CO) = E_{slab+CO} - E_{slab} - E_{CO}$, where E_{slab} and $E_{slab+CO}$ stand for the total energies of the slab without and with the CO, and E_{CO} is the total energy of CO molecule. The adsorption energy of OH on metal surfaces were defined as $E_{ads}(OH) = E_{slab+OH} - E_{slab} - (E_{H_2O} - \frac{1}{2}H_2)$, where E_{slab} and $E_{slab+OH}$ stand for the total energies of the slab without and with the OH, and E_{H_2} and E_{H_2O} account for the total energies of the hydrogen and water molecules in the gaseous state, respectively.

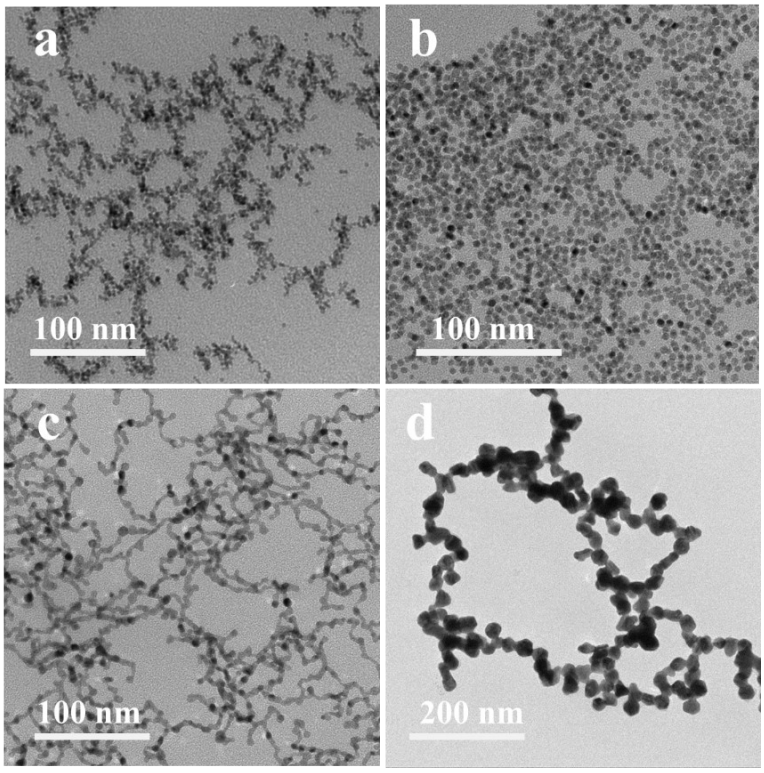

Fig. S1 TEM images of PdBiPt NWs with different usage of bismuth triacetate precursors: (a) 0, (b) 1, (c) 2, and (d) 5 mg.

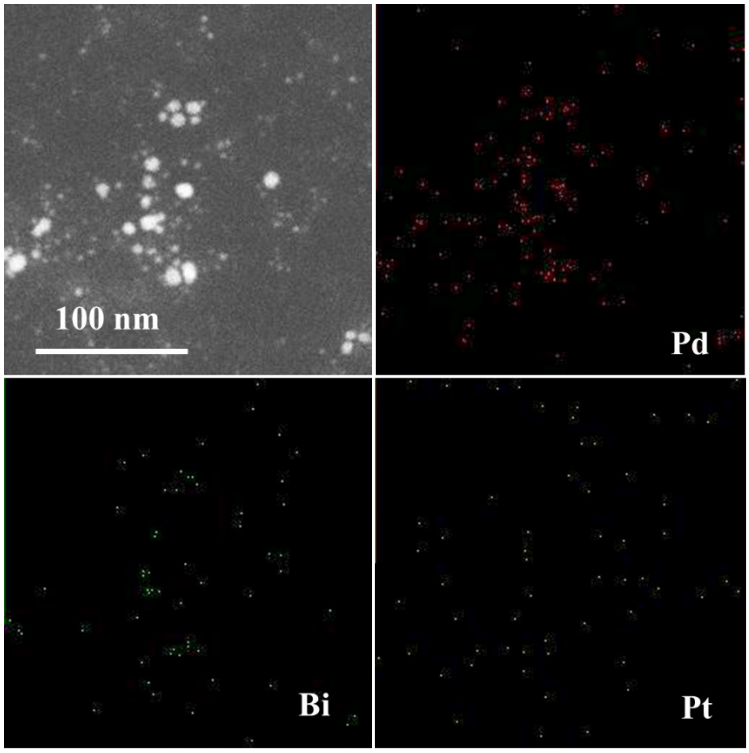

Fig. S2 Elemental mapping images of PdBiPt nanoparticles with the reaction time of 5 mins.

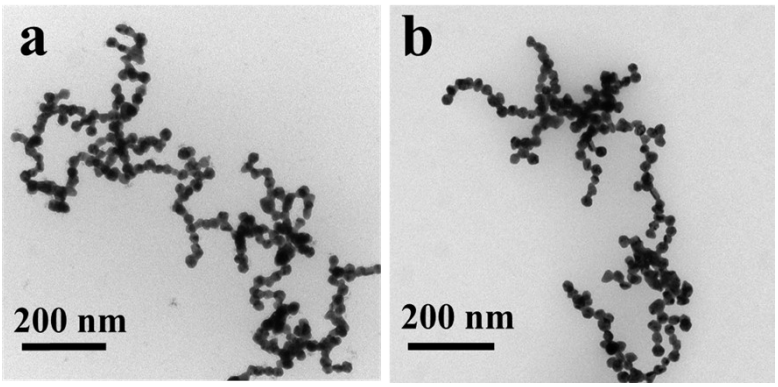

Fig. S3 TEM images of PdBi NWs (a) and PdBiPt NWs (b) by replacing Na_2PdCl_4 with $Pd(acac)_2$ precursors.

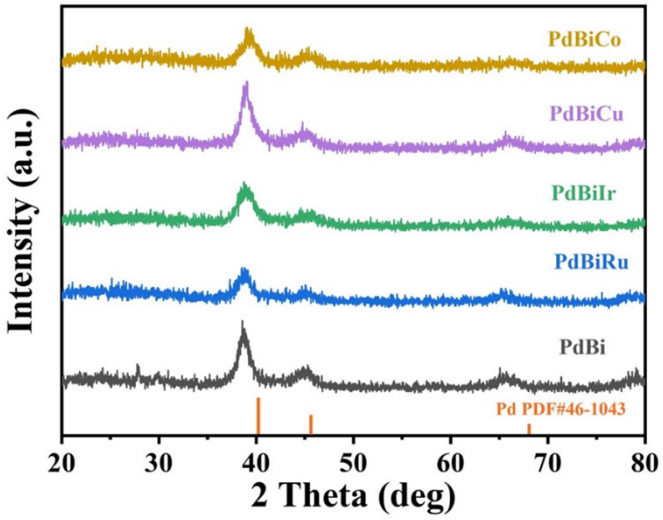

Fig. S4 XRD patterns of PdBiCo, PdBiCu, PdBiIr, PdBiRh, and PdBi NWs.

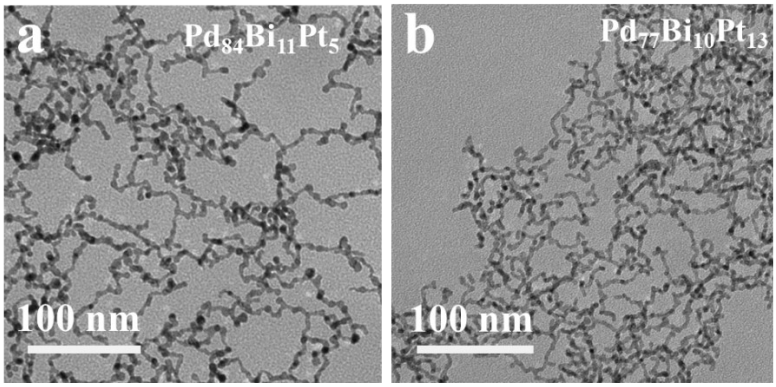

Fig. S5 TEM images of PdBiPt NWs with different usage of $Pt(acac)_2$ precursors: (a) 1 and (b) 3 mg.

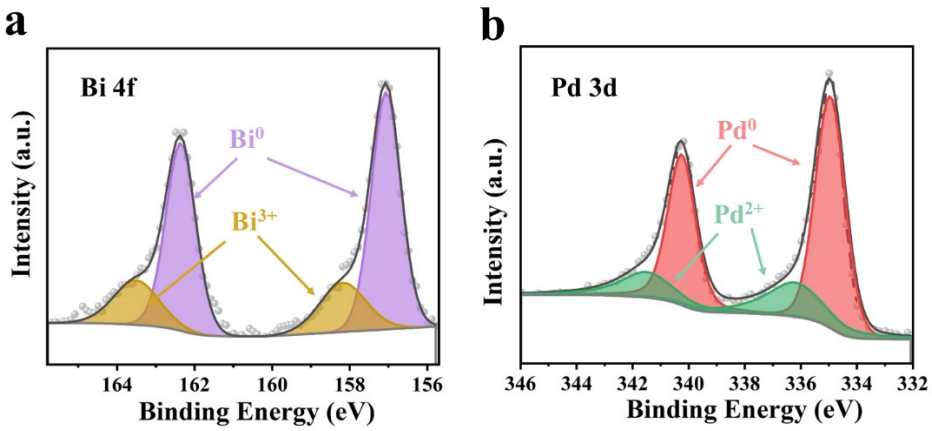

Fig. S6 XPS spectra of Bi 4f (a) and Pd 3d (b) for PdBi NWs.

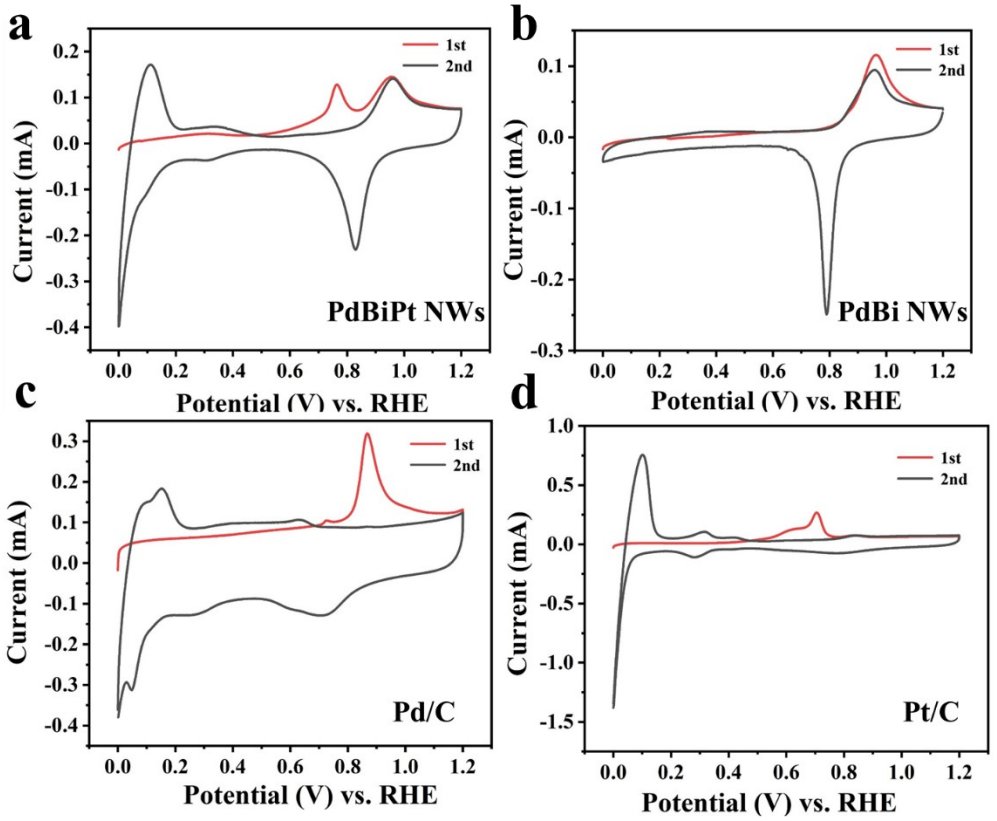

Fig. S7 CO-stripping curves of (a) PdBiPt NWs, (b) PdBi NWs, (c) Pd/C, and (d) Pt/C.

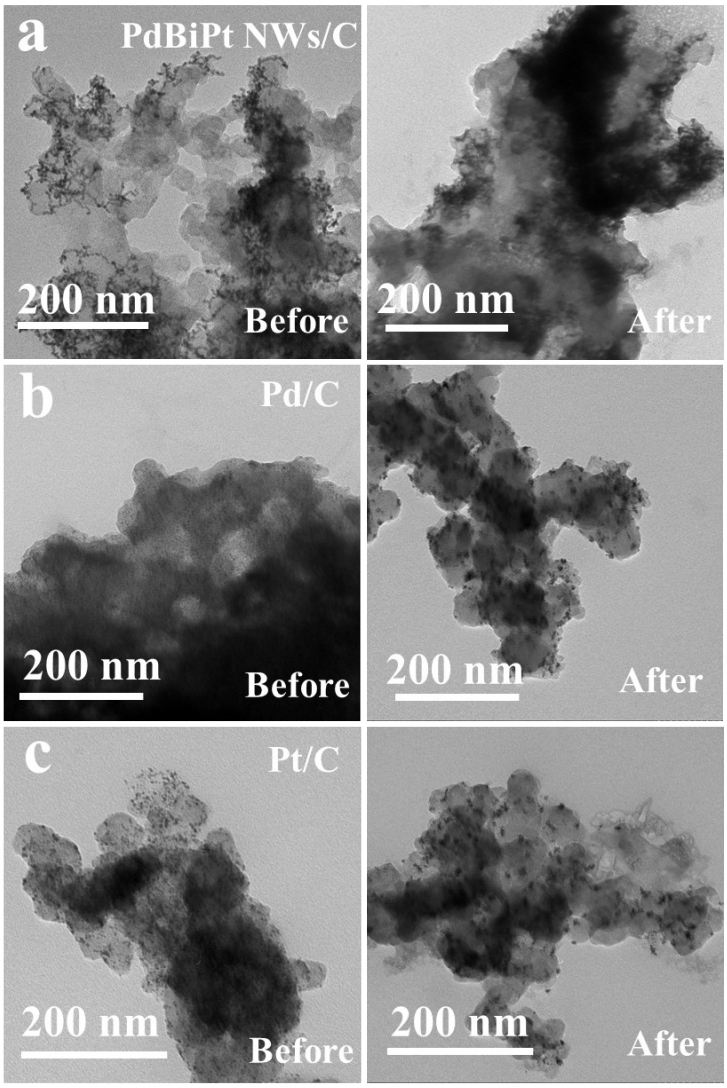

Fig. S8 TEM images of structure characterizations before and after durability test of PdBiPt NWs/C (a), Pd/C (b), and Pt/C (c).

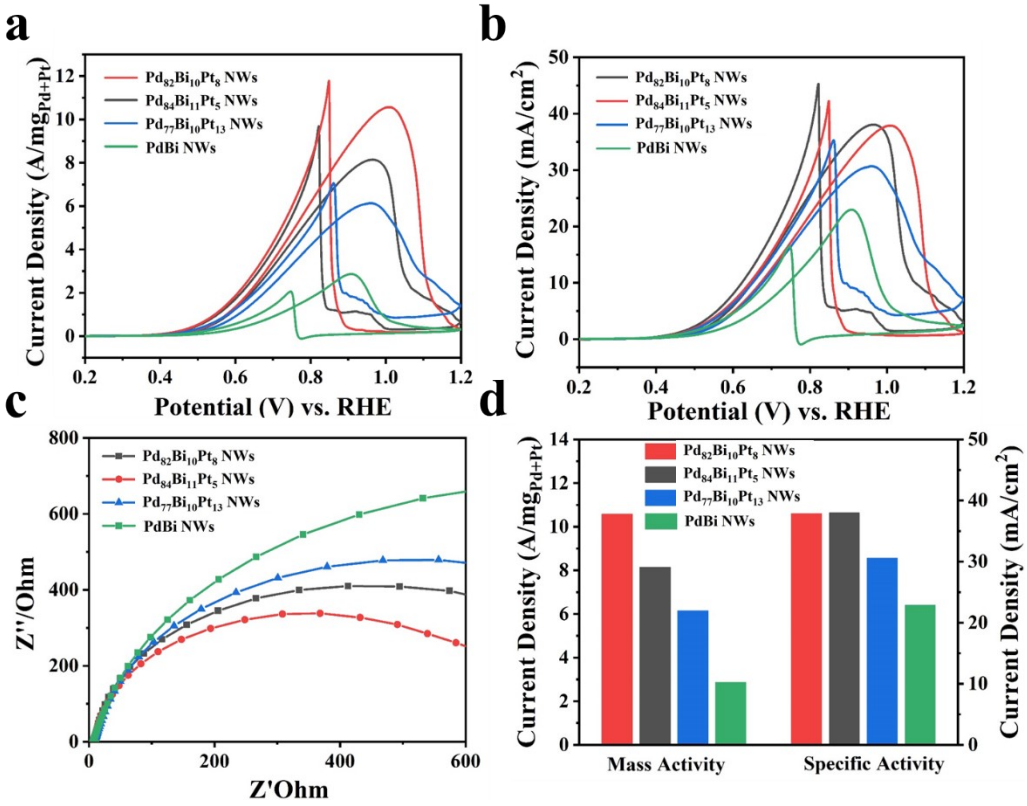

Fig. S9 EOR performance of PdBiPt NWs with different compositions. Mass-normalized (a) and ECSA-normalized (b) EOR CV curves in 1.0 M KOH and 1.0 M ethanol. (c) Nyquist plots of these catalysts. (d) Mass and specific activities of PdBiPt NWs, PdBi NWs, Pd/C and Pt/C.

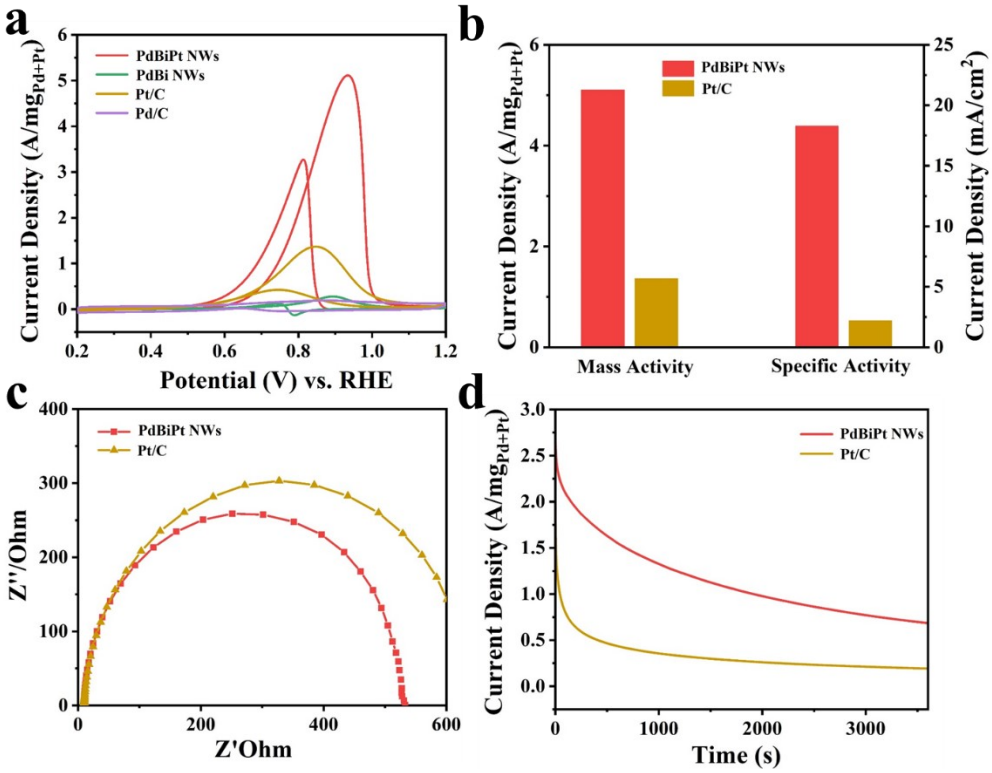

Fig. S10 Electrocatalytic MOR of PdBiPt NWs, PdBi NWs and Pt/C. (a) Mass-normalized MOR CV curves in 1.0 M KOH and 1.0 M methanol. (b) Mass and specific activities of PdBiPt NWs, PdBi NWs and Pt/C. (c) Nyquist plots of these catalysts. (d) i-t curves of these catalysts at 0.8 V.

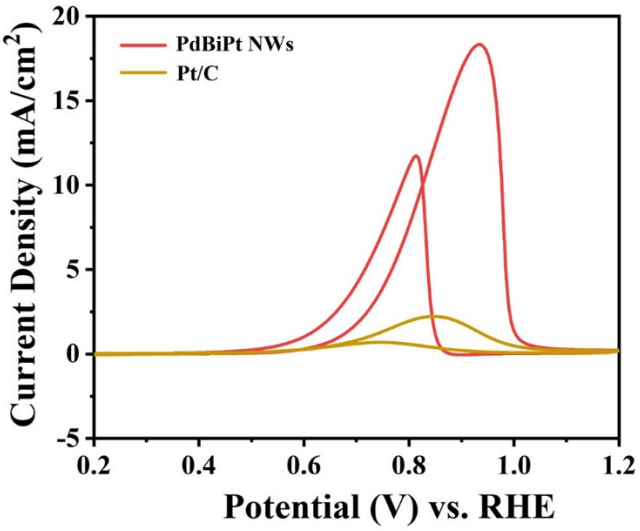

Fig. S11 ECSA-normalized MOR CV curves.

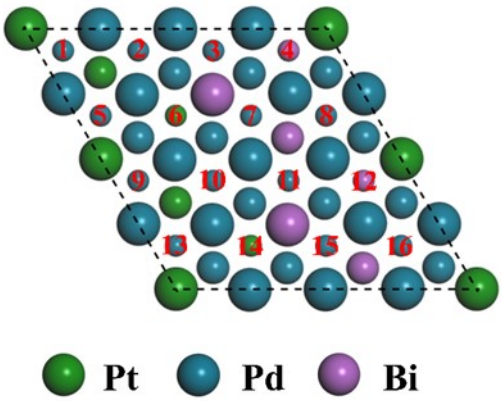

Fig. S12 Top views of PdBiPt NW (111) surface in DFT calculations. The numbers indicated the possible absorption sites of *CO and *OH considered in our DFT calculations.

Table S1. EOR performance of the state-of-the-art catalysts.

Catalyst	Mass Activity (A/mg_{metal})	Specific Activity (mA/cm^2)	Electrolyte	Reference
PdBiPt NWs	10.57	27.92	1MKOH+1MC_2H_5OH	This work
PtRuRhCoNi NWs/C	7.68	7.55	1MKOH+1MC_2H_5OH	1[7]
PtBi@$PtRh_1$	13.00	/	1MKOH+1MC_2H_5OH	2[8]
Au@Pd	6.82	11.03	1MKOH+1MC_2H_5OH	3[9]
Pd_2Ag_1 sNWs	2.84	11.20	1MKOH+1MC_2H_5OH	4[10]
Pd_6Pb_1	2.34	/	1MKOH+1MC_2H_5OH	5[11]
PdBP NWs@N-G	4.15	/	1MKOH+1MC_2H_5OH	6[12]
Pt_3Ag NWs	6.10	28.00	1MKOH+1MC_2H_5OH	7[13]
$AuPt_3$	6.67	17.59	1MKOH+1MC_2H_5OH	8[14]
PtCu/$Cu_{2-x}Se$ NWs	5.03	7.68	1MKOH+1MC_2H_5OH	9[15]
PdAgAu NWs	2.40	5.5	1MKOH+1MC_2H_5OH	10[16]

Table S2. The calculated adsorption energies of *CO and *OH adsorbed on different surface sites of PdBiPt NW (111) are shown in Figure S11.

No.	E_{ads} (CO) /eV	E_{ads} (OH) /eV
1	-2.15	0.75
2	/	0.70
3	/	0.76
4	-2.10	0.60
5	-2.15	0.61
6	/	0.78
7	-1.95	0.65
8	-2.10	0.59
9	-2.15	0.75
10	-1.80	0.70
11	/	0.76
12	-2.10	0.60
13	-2.15	0.61
14	/	0.77
15	-1.95	0.65
16	-2.10	0.59

References

1. G. Kresse and D. Joubert, *Physical Review B*, 1999, **59**, 1758-1775.
2. G. Kresse and J. Hafner, *Physical Review B*, 1994, **49**, 14251-14269.
3. G. Kresse and J. Furthmüller, *Physical Review B*, 1996, **54**, 11169-11186.
4. J. P. Perdew, K. Burke and M. Ernzerhof, *Physical review letters*, 1996, **77**, 3865-3868.
5. S. Grimme, *Journal of Computational Chemistry*, 2006, **27**, 1787-1799.
6. H. J. Monkhorst and J. D. Pack, *Physical Review B*, 1976, **13**, 5188-5192.

7. H. D. Li, M. Z. Sun, Y. Pan, J. Xiong, S. H. Feng, Z. J. Li, J. P. Lai, B. L. Huang and L. Wang, *Appl Catal B-Environ*, 2022, **312**, 121431.
8. S. Luo, L. Zhang, Y. Liao, L. Li, Q. Yang, X. Wu, X. Wu, D. He, C. He, W. Chen, Q. Wu, M. Li, E. J. M. Hensen and Z. Quan, *Adv. Mater.*, 2021, **33**.
9. X. Zhou, Y. Ma, Y. Ge, S. Zhu, Y. Cui, B. Chen, L. Liao, Q. Yun, Z. He, H. Long, L. Li, B. Huang, Q. Luo, L. Zhai, X. Wang, L. Bai, G. Wang, Z. Guan, Y. Chen, C.-S. Lee, J. Wang, C. Ling, M. Shao, Z. Fan and H. Zhang, *Journal of the American Chemical Society*, 2021, **144**, 547-555.
10. H. Lv, Y. Wang, A. Lopes, D. Xu and B. Liu, *Appl. Catal. B-Environ.*, 2019, **249**, 116-125.
11. F. H. Gao, B. Fu, L. Y. Xu, L. K. Yang and P. Z. Guo, *Chemnanomat*, 2022, **8**.
12. H. Lv, L. Sun, D. Xu and B. Liu, *Science Bulletin*, 2020, **65**, 1823-1831.
13. X. Fu, C. Wan, A. Zhang, Z. Zhao, H. Huyan, X. Pan, S. Du, X. Duan and Y. Huang, *Nano Research*, 2020, **13**, 1472-1478.
14. Z. He, Q. Duan, L. Liao and C. Wang, *Chem. Eng. J*, 2023, **468**, 143411.
15. H. Peng, J. Ren, Y. Wang, Y. Xiong, Q. Wang, Q. Li, X. Zhao, L. Zhan, L. Zheng, Y. Tang and Y. Lei, *Nano Energy*, 2021, **88**, 106307.
16. H. Wang, S. Jiao, S. Liu, K. Deng, H. Yu, X. Wang, Y. Xu, Z. Wang and L. Wang, *J. Mater. Chem. A*, 2022, **10**, 24051-24055.